frontiers in Physics

ORIGINAL RESEARCH
published: 14 December 2021
doi: 10.3389/fphy.2021.698154

Asymmetric Interfacial Intermixing Associated Magnetic Coupling in $LaMnO_3/LaFeO_3$ Heterostructures

Binbin Chen[1], *Nicolas Gauquelin*[2], *Robert J. Green*[3,4], *Johan Verbeeck*[2], *Guus Rijnders*[1] *and Gertjan Koster*[1]*

[1]*MESA+ Institute for Nanotechnology, University of Twente, Enschede, Netherlands,* [2]*Electron Microscopy for Materials Science (EMAT), University of Antwerp, Antwerp, Belgium,* [3]*Department of Physics and Engineering Physics, University of Saskatchewan, Saskatoon, SK, Canada,* [4]*Stewart Blusson Quantum Matter Institute, University of British Columbia, Vancouver, BC, Canada*

The structural and magnetic properties of $LaMnO_3/LaFeO_3$ (LMO/LFO) heterostructures are characterized using a combination of scanning transmission electron microscopy, electron energy-loss spectroscopy, bulk magnetometry, and resonant x-ray reflectivity. Unlike the relatively abrupt interface when LMO is deposited on top of LFO, the interface with reversed growth order shows significant cation intermixing of Mn^{3+} and Fe^{3+}, spreading ~8 unit cells across the interface. The asymmetric interfacial chemical profiles result in distinct magnetic properties. The bilayer with abrupt interface shows a single magnetic hysteresis loop with strongly enhanced coercivity, as compared to the LMO plain film. However, the bilayer with intermixed interface shows a step-like hysteresis loop, associated with the separate switching of the "clean" and intermixed LMO sublayers. Our study illustrates the key role of interfacial chemical profile in determining the functional properties of oxide heterostructures.

Keywords: oxide interface, asymmetric cation intermixing, thin film growth, enhanced magnetic coercivity, ferromagnetism

OPEN ACCESS

Edited by:
Matjaž Spreitzer,
Institut Jožef Stefan (IJS), Slovenia

Reviewed by:
Nini Pryds,
Technical University of Denmark, Denmark
Felix Gunkel,
Helmholtz Association of German Research Centres (HZ), Germany

***Correspondence:**
Gertjan Koster
g.koster@utwente.nl

Specialty section:
This article was submitted to Physical Chemistry and Chemical Physics, a section of the journal Frontiers in Physics

Received: *24 April 2021*
Accepted: *24 November 2021*
Published: *14 December 2021*

Citation:
Chen B, Gauquelin N, Green RJ, Verbeeck J, Rijnders G and Koster G (2021) Asymmetric Interfacial Intermixing Associated Magnetic Coupling in $LaMnO_3/LaFeO_3$ Heterostructures. Front. Phys. 9:698154. doi: 10.3389/fphy.2021.698154

INTRODUCTION

Controlling the magnetic interactions across heterointerfaces play a central role in spintronics [1]. Due to the entangled spin, orbital, charge, and lattice degrees of freedom in transition metal oxides, the magnetic interactions at oxide interfaces are complicated by the presence of epitaxial strain, oxygen octahedral coupling, charge transfer, orbital hybridization, electron confinement, etc [2–5]. A well-known phenomenon related to the interfacial magnetic coupling is exchange bias (EB), which usually occurs in field-cooled ferromagnetic/antiferromagnetic systems [6]. EB is characterized by a horizontal shift of the magnetic hysteresis loop along with an enhanced coercive field (H_C), and is usually interpreted by the pinning effect from uncompensated surface spins of the antiferromagnetic material. For a fully compensated antiferromagnetic surface, such as the (001) plane of a G-type antiferromagnet, a spin-flop coupling is energetically favorable [7]. The antiferromagnetic spin axis aligns perpendicular to the ferromagnetic spins to minimize the interfacial spin frustration, as revealed at $La_{0.7}Sr_{0.3}MnO_3/La(Sr)FeO_3$ interfaces [8–10]. Normally such spin-flop coupling is unable to induce EB, but only increases H_C, while extrinsic disorders (interface roughness, for example) can create random fields acting on the ferromagnetic spins and cause EB [11,12]. Also, an intrinsic mechanism involving Dzyaloshinskii-Moriya interaction has been proposed to explain the EB at ferromagnetic/G-type antiferromagnetic interface [10,13]. In particular, it has been reported that the orbital hybridization and superexchange interaction between Mn and Fe at the interface of $La_{2/3}Sr_{1/}$

$_3MnO_3/BiFeO_3$ gave rise to a spin-canted state of Fe^{3+} and a concomitant EB effect [14–16]. However, first-principles calculations ascribe the magnetism of Fe^{3+} to the interfacial Mn/Fe chemical intermixing [17], which is supported by the absence of EB at the chemically abrupt interface [16]. These results point to the crucial role of interfacial chemical profile in dictating the magnetic coupling across oxide interfaces.

Pulsed laser deposition (PLD) has been widely used to construct oxide interfaces. Although tremendous achievements have been made in this field over the past few decades, the abruptness across oxide interfaces remains a controversial issue [18]. The high temperature required for the epitaxial growth as well as the high-energy species generated in the laser plume naturally facilitate the inter-diffusion between two adjoined layers [19,20]. The resulted composition variation can profoundly influence the interface properties by introducing disorders, distorting the local structure and/or altering the valence states [16,21–24]. In this work, the effects of interfacial cation interdiffusion on the magnetic properties of $LaMnO_3$/$LaFeO_3$ (LMO/LFO) heterostructures have been studied using a combination of atomically resolved scanning transmission electron microscopy (STEM), electron energy-loss spectroscopy (EELS), bulk magnetometry and resonant x-ray reflectivity (RXR). In particular, the degree of Mn/Fe intermixing is found to depend on the growth sequence, i.e., the LMO-on-LFO interface is relatively sharp, while the LFO-on-LMO interface shows pronounced Mn/Fe intermixing over ~8 unit cells (uc) of the interfacial region. Such structural asymmetry is further manifested by the distinct magnetic properties of the two bilayers.

MATERIALS AND METHODS

The LMO/LFO bilayers were fabricated on TiO_2-terminated $SrTiO_3$ (001) substrates using PLD, *in situ* monitored by reflection high energy electron diffraction (RHEED). In order to achieve TiO_2-terminated and terraced surface, the $SrTiO_3$ substrates were first etched with buffered hydrofluoric acid, followed by annealing in flowing oxygen at 1050°C for 2 h. During the PLD deposition, the substrate temperature and oxygen pressure were maintained at 700°C and 0.01 mbar, respectively. The laser fluence and repetition rate were set at 1.8 J/cm^2 and 2 Hz, respectively. The surface morphology was verified using atomic force microscopy (AFM). The atomic resolution monochromated STEM-EELS was acquired on a Thermofisher Scientific Titan electron microscope, equipped with Cs-correction for the probe and an Enfinium spectrometer, operated at 300 kV. The bulk magnetic properties were measured using vibrating sample magnetometry on a Quantum Design physical property measurement system. The RXR experiments were performed using an in-vacuum 4-circle diffractometer at the Resonant Elastic and Inelastic X-ray Scattering (REIXS) beamline of the Canadian Light Source (CLS) in Saskatoon, Canada [25]. The measurements were carried out at 20 K with a specular reflection geometry.

RESULTS AND DISCUSSION

Bulk LMO is an A-type antiferromagnet with antiparallel aligned ferromagnetic planes [26]. When grown on $SrTiO_3$, it adopts a ferromagnetic state due to the electronic reconstruction and/or oxygen non-stoichiometry [27–30]. Bulk LFO is a typical G-type antiferromagnet with a Néel temperature (T_N) up to 740 K [31]. The antiferromagnetism can be retained in its thin-film form down to a thickness of 3 uc [32]. Here, LMO_m/LFO_n bilayers have been grown on TiO_2-terminated $SrTiO_3$ (001) substrates using PLD, with subscripts m and n indicating the corresponding layer thickness in uc. **Figure 1A** shows the surface morphologies of two bilayers with reversed stacking sequence, LMO_{10}-on-LFO_{12} and LFO_{12}-on-LMO_{10} as sketched in the insets. Both samples show atomically flat surfaces with step terraces of one uc in height, in accordance with the layer-by-layer growth mode observed in RHEED (**Supplementary Figure S1**).

The magnetic properties of the two samples are compared in **Figures 1B,C**, together with those of 10-uc LMO and 12-uc LFO plain films for reference. The LFO film is antiferromagnetic showing no magnetic signal, while the LMO film is ferromagnetic with a Curie temperature (T_C) of ~140 K and saturation magnetization (M_S) of ~2.1 μ_B/Mn at 10 K. When LMO is deposited on top of an LFO buffer layer, T_C remains unchanged, but M_S drops to 1.6 μ_B/Mn. The reduced magnetization can be understood by magnetic frustrations at the ferromagnetic/G-antiferromagnetic interface with competing exchange interactions, as suggested in $La_{0.6}Sr_{0.4}MnO_3$/$La_{0.6}Sr_{0.4}FeO_3$ superlattices [33]. It is interesting to note that the T_C is unaltered by the magnetic frustrations here, which is probably due to the relatively thick LMO layer as well as the heterogenous magnetic states of LMO [34]. Moreover, Gibert et al. reported a canted antiferromagnetic state in LMO grown on a $LaNiO_3$ buffer layer, which has been ascribed to the modifications of Mn-O-Mn bond angles induced by $LaNiO_3$ [24]. Such an effect may also play a role in the suppressed magnetization of the LMO-on-LFO bilayer, given the strong octahedral rotations in the orthorhombic LFO. As can be seen in **Figure 1C**, the LMO-on-LFO bilayer shows H_C ~ 890 Oe, much larger than the LMO single film with H_C ~ 340 Oe. Meanwhile, no EB was observed after cooling to 10 K in a field of 1T (**Figure 1D**). These observations agree with a spin-flop coupling proposed for ferromagnetic/G-antiferromagnetic systems [12]. For the LFO-on-LMO bilayer, the temperature dependent magnetization curve shows drastically reduced T_C and M_S, as compared to the LMO film. More strikingly, a step-like hysteresis loop was observed (**Figure 1C**), indicating two separate magnetic switching events during the field sweeping. Similar behavior has also been observed with different layer thickness of LMO (**Supplementary Figure S2**) This is in stark contrast with the LMO-on-LFO bilayer. As we will show below, the distinct behaviors are associated with the asymmetric Mn/Fe intermixing at the interface, which depends on the stacking sequence.

Figures 2A,C show the STEM-EELS elemental maps of the LFO_{12}-on-LMO_7 and LMO_{10}-on-LFO_{12} bilayers, respectively. The corresponding layer-resolved EELS intensities of La, Sr,

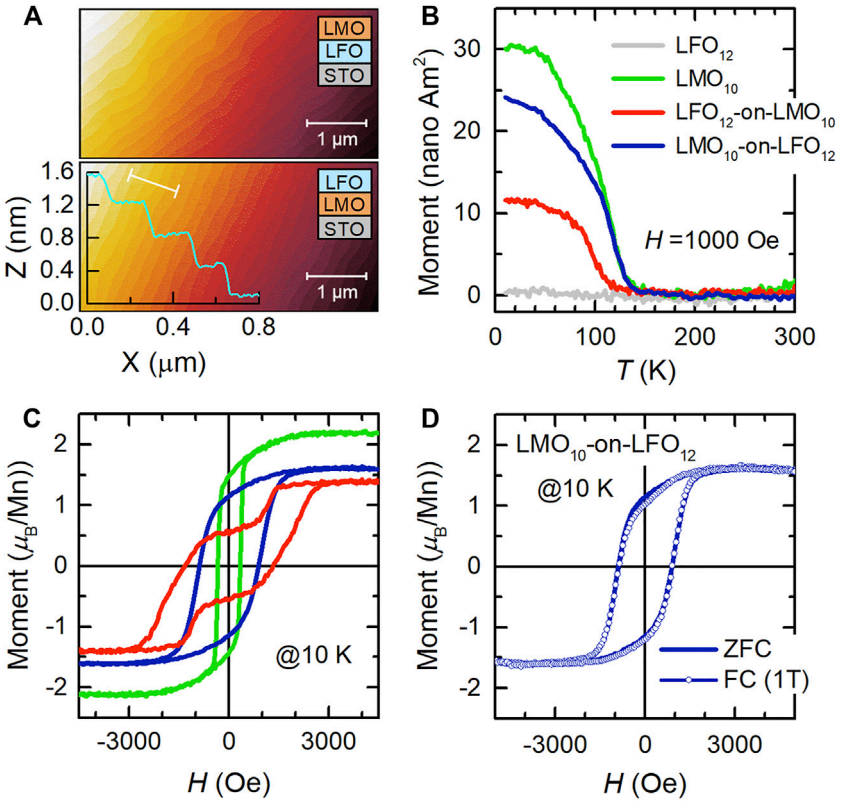

FIGURE 1 | (A) AFM images of LMO_{10}-on-LFO_{12} and LFO_{12}-on-LMO_{10} bilayers with reversed stacking sequence. The inset of bottom panel shows the height profile along the white line. **(B)** Temperature dependent magnetization curves of the LMO_{10}, LFO_{12} single films, and LMO_{10}-on-LFO_{12}, LFO_{12}-on-LMO_{10} bilayers, measured with a cooling field of 1000 Oe. **(C)** shows the corresponding magnetic hysteresis loops at 10 K. The magnetic moments were caluculated using only the volume of LMO. **(D)** Magnetic hysteresis loops of LMO_{10}-on-LFO_{12} measured after zero field cooling (ZFC) and 1-T field cooling (FC) to 10 K.

Ti, Mn, and Fe are plotted in the upper panels of **Figures 2B,D**. For the LFO_{12}-on-LMO_7 interface, a strong cation intermixing of Mn and Fe ions is observed, spanning ~8 uc across the interface. This is similar to what was observed in the LFO-on-LMO bilayer grown by molecular beam epitaxy [35]. In contrast, the LMO_{10}-on-LFO_{12} interface is relatively sharp, with Mn/Fe intermixing confined within ~2 uc at the interface. Such an asymmetric chemical profile has also been reported in the heterostructures of $LaVO_3$/STO and LMO/$LaNiO_3$, where the diffuse interfaces are interpreted by preferential ionic surface segregations driven by the difference in the ion radii [24,36]. However, this scenario should not be at play for the LMO/LFO interface considering the identical ionic radii of Mn^{3+} and Fe^{3+} [37]. Further theoretical studies are needed to address the puzzling interdiffusion behavior at the LMO/LFO interface by taking into accounts the interface energy and surface energies of LMO and LFO. By fitting the EELS spectra of Mn (Fe) $L_{2,3}$ edge to references of Mn^{2+} and Mn^{3+} (Fe^{2+} and Fe^{3+}), the layer-resolved valence states of Mn and Fe were obtained and plotted in the bottom panels of **Figures 2B,D**. Apparently, no charge transfer between Mn^{3+} and Fe^{3+} occurs in both heterostructures, in line with the previous report [35]. The presence of Mn^{2+} at the LMO/STO interface (**Figure 2B**) is due to electron accumulation driven by the polar discontinuity [28,29,38]. In contrast, no electronic reconstructions are observed at the LFO/STO interface because of the stable $3d^5$ electronic configuration of Fe^{3+} [39]. Instead, Nakamura et al. showed that the polar charges were screened by an emergent spontaneous polarization at the LFO/STO heterointerface [40]. Overall, our STEM measurements demonstrate the LMO-on-LFO interface being chemically sharper than the LFO-on-LMO interface, and preclude any charge transfer between LMO and LFO.

RXR measurements were performed on a LFO_{12}-on-LMO_{10} bilayer to gain insights into the step-like magnetic switching behavior. X-ray reflectivity at off-resonant energies were first measured to extract the chemical depth profile. By tuning the x-ray energy to the Mn and Fe resonances, the depth profiles of Mn and Fe magnetization can be extracted independently. In general the on-resonance x-ray reflectivity for a particular element provides an enhanced sensitivity to the depth profile of the density of that element. On resonance, the enhanced refractive index generally leads to stronger contrast in the constructive/destructive interference in x-ray reflectivity. **Figure 3A** shows the x-ray reflectivity at off-resonant energies (455, 633, 698, and 841 eV). The atomic concentrations of Ti, Mn, and Fe are extracted from the simulations and shown in **Figure 3C**. The Mn and Fe intermix over ~7 uc around the interface, in good agreement with the STEM results. In order to

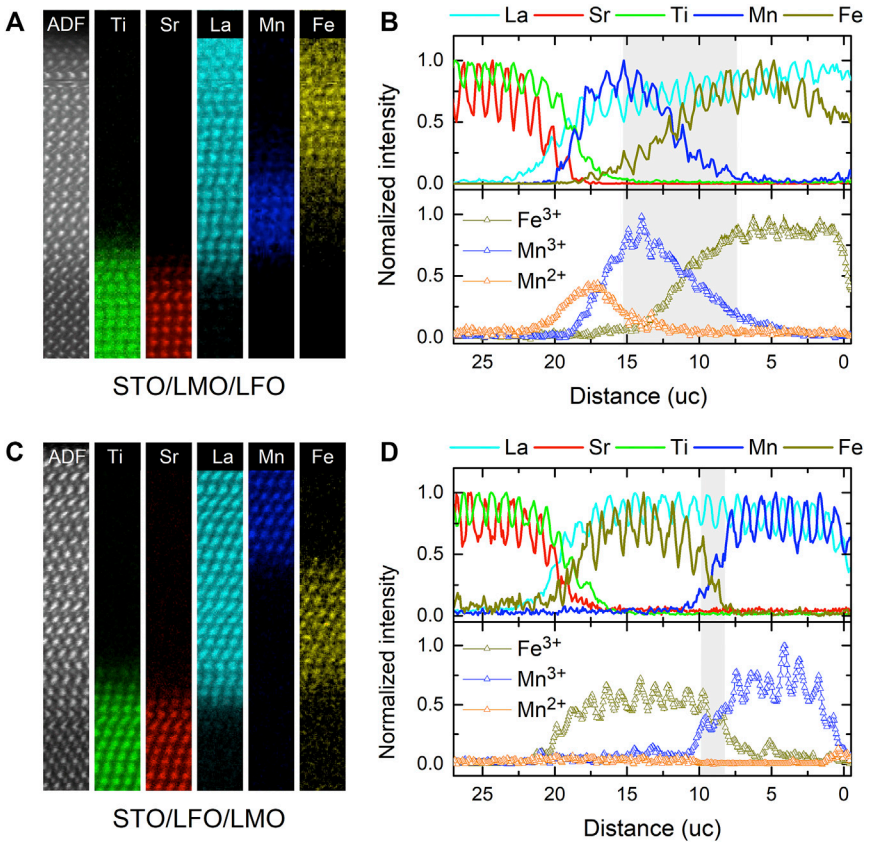

FIGURE 2 | (A,C) STEM-EELS elemental maps of Ti $L_{2,3}$, Sr $L_{2,3}$, La $M_{4,5}$, Mn $L_{2,3}$, Fe $L_{2,3}$, along with the simutaneously acquired annular dark field (ADF) images measured for the LFO_{12}-on-LMO_7 and LMO_{10}-on-LFO_{12} bilayers, respectively. The corresponding layer-resolved EELS intensities and valence states (Mn and Fe) are shown in **(B)** and **(D)**, respectively.

resolve the magnetic switching process, RXR measurements were performed at both saturation (0.6 T) and remanence (Rem) states using circularly left (R_L) and right (R_R) polarized light. The asymmetry curves $(R_L\text{-}R_R)/(R_L+R_R)$ measured at the L_3 edges of Mn (641 eV) and Fe (710 eV) are depicted in **Figure 3B**, and the derived magnetic depth profiles are shown in **Figure 3D**. By applying a field of 0.6 T, we observed a pronounced Fe magnetization in the intermixed region, which peaked around Z ~ 40 Å. According to Goodenough-Kanamori-Anderson rules, the superexchange interaction between Mn^{3+} (t_{2g}^3,e_g^1) and Fe^{3+} (t_{2g}^3,e_g^2) are strongly ferromagnetic [41–43]. Thus, the Fe moments can be induced by interacting with the surrounding Mn^{3+} ions [17]. The Fe magnetization is limited by the small volume fraction of Fe ions for $Z < 40$ Å, while the increasing Fe-O-Fe antiferromagnetic interactions suppress the magnetization for $Z > 40$ Å. Surprisingly, the Fe moments vanished as the magnetic field was removed. This might correspond to a magnetic cluster (or superparamagnetic) state in the intermixed $LaMn_{1-x}Fe_xO_3$ [44], whose magnetization becomes randomly aligned at zero fields. Notably, the magnetization of Mn is also depressed to a great extent after removing the magnetic field, even in the region without significant Mn/Fe intermixing. This means that some domains are already reversed at zero fields in LMO. Based on our RXR results, the magnetic switching sequences are sketched in **Figure 3E**. The step-like hysteresis loop observed for the LFO_{12}-on-LMO_{10} bilayer corresponds to the separating switching of the intermixed $LaMn_{1-x}Fe_xO_3$ and the "clean" LMO sublayers.

To further ascertain the above scenario, we used $LaAlO_3$ as a shielding layer to prohibit the interfacial intermixing between LMO and LFO. As shown in **Figure 4**, the F-A-M trilayer exhibits a very similar behavior to the LMO single film, with slightly higher T_C and M_S. In contrast, a considerably larger M_S was observed for the M-A-F trilayer at low temperature, implying the significant role of capping layer in enhancing the magnetization of LMO [45]. Furthermore, the three samples show slim loops at 10 K with the same H_C ~ 400 Oe, ruling out any exchange couplings at the interface. The single loop of the M-A-F trilayer strongly suggests that the step-like switching behavior is associated with the LFO/LMO interface.

CONCLUSION

To summarize, we demonstrate an asymmetric interdiffusion at the interface between LMO and LFO, which depends on the growth sequence. The LMO-on-LFO bilayer with relatively sharp

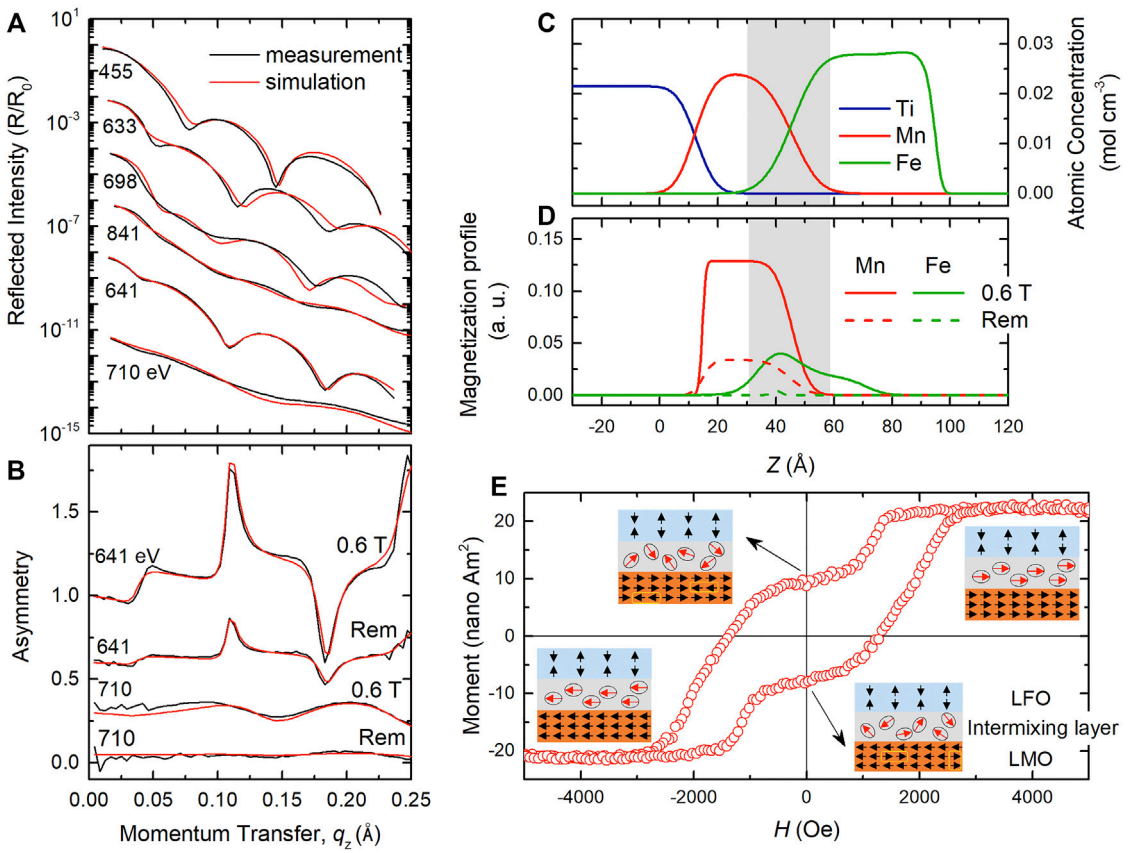

FIGURE 3 | (A) X-ray reflectivity curves of the LFO_{12}-on-LMO_{10} bilayer at 20 K using varied phonon energies. **(B)** Magnetic asymmetry of the saturation (0.6 T) and remenance (Rem) states measured at the L_3 edges of Mn (641 eV) and Fe (710 eV). **(C,D)** Chemical and magnetization profiles derived from the off-resonant and resonant RXR measurements. **(E)** Schematics of the magnetization swiching process.

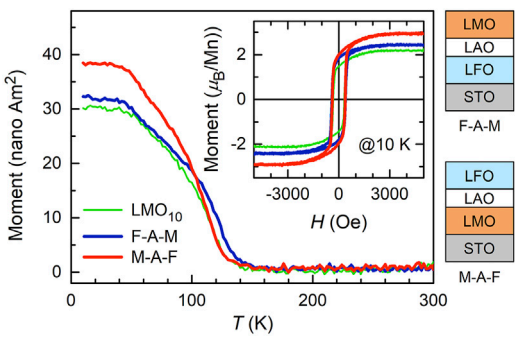

FIGURE 4 | Temperature dependent magnetization curves of the 10-uc LMO single film, $LFO_{12}/LAO_4/LMO_{10}$ (F-A-M) and $LMO_{10}/LAO_4/LFO_{12}$ (M-A-F) trilayers measured under a cooling field of 1000 Oe. Inset shows the corresponding magnetic hysteresis loops recorded at 10 K. The structures of F-A-M and M-A-F are schematically drawn on the right.

interface shows a single magnetic hysteresis loop with enhanced H_C as compared to the referenced LMO film. However, for the LFO-on-LMO case, the interfacial layer with strong Mn/Fe intermixing constitutes an extra magnetic phase. This phase switches separately from the LMO layer, yielding a step-like magnetic hysteresis loop. We further show that the strong interdiffusion at LFO-on-LMO interface can be prohibited by inserting a $LaAlO_3$ shielding layer. Future experiments, to elucidate on the mechanisms as well as control of interdiffusion, should include the insertion of thin buffer layers, change of the substrate terminations, variations of the thicknesses and finally deposition parameters. Our results call for more investigations into the interfacial chemical profile to interpret those emergent phenomena at complex oxide interfaces.

DATA AVAILABILITY STATEMENT

The raw data supporting the conclusion of this article will be made available by the authors, without undue reservation.

AUTHOR CONTRIBUTIONS

BC and GK conceived the research. BC grew the samples and performed the basic structural and magnetic characterizations. NG performed the STEM measurements and data analysis under

the supervision of JV. RG performed the RXR measurements and the signal simulations. BC and GK wrote the paper with input from all authors.

FUNDING

This work is supported by the international M-ERA.NET project SIOX (project 4288) and H2020 project ULPEC (project 732642). The X-Ant-EM microscope and the direct electron detector were partly funded by the Hercules fund from the Flemish Government. NG and JV acknowledge funding from GOA project "Solarpaint" of the University of Antwerp. RG was supported by the Natural Sciences and Engineering Research Council of Canada (NSERC). Part of the research described in this paper was performed at the Canadian Light Source, a national research facility of the University of Saskatchewan, which is supported by the Canada Foundation for Innovation (CFI), NSERC, the National Research Council (NRC), the Canadian Institutes of Health Research (CIHR), the Government of Saskatchewan, and the University of Saskatchewan.

SUPPLEMENTARY MATERIAL

The Supplementary Material for this article can be found online at: https://www.frontiersin.org/articles/10.3389/fphy.2021.698154/full#supplementary-material

REFERENCES

1. Wolf SA, Awschalom DD, Buhrman RA, Daughton JM, von Molnár S, Roukes ML, et al. Spintronics: A Spin-Based Electronics Vision for the Future. *Science* (2001) 294:1488–95. doi:10.1126/science.1065389
2. Zubko P, Gariglio S, Gabay M, Ghosez P, Triscone J-M. Interface Physics in Complex Oxide Heterostructures. *Annu Rev Condens Matter Phys* (2011) 2: 141–65. doi:10.1146/annurev-conmatphys-062910-140445
3. Hwang HY, Iwasa Y, Kawasaki M, Keimer B, Nagaosa N, Tokura Y. Emergent Phenomena at Oxide Interfaces. *Nat Mater* (2012) 11:103–13. doi:10.1038/nmat3223
4. Bhattacharya A, May SJ. Magnetic Oxide Heterostructures. *Annu Rev Mater Res* (2014) 44:65–90. doi:10.1146/annurev-matsci-070813-113447
5. Liao Z, Huijben M, Zhong Z, Gauquelin N, Macke S, Green RJ, et al. Controlled Lateral Anisotropy in Correlated Manganite Heterostructures by Interface-Engineered Oxygen Octahedral Coupling. *Nat Mater* (2016) 15:425–31. doi:10.1038/NMAT4579
6. Nogués J, Schuller IK. Exchange Bias. *J Magnetism Magn Mater* (1999) 192: 203–32. doi:10.1016/S0304-8853(98)00266-2
7. Koon NC. Calculations of Exchange Bias in Thin Films with Ferromagnetic/Antiferromagnetic Interfaces. *Phys Rev Lett* (1997) 78:4865–8. doi:10.1103/PhysRevLett.78.4865
8. Arenholz E, Van Der Laan G, Yang F, Kemik N, Biegalski MD, Christen HM, et al. Magnetic Structure of La0.7Sr0.3MnO3/La0.7Sr0.3FeO3 Superlattices. *Appl Phys Lett* (2009) 94:072503. doi:10.1063/1.3085765
9. Folven E, Scholl A, Young A, Retterer ST, Boschker JE, Tybell T, et al. Crossover from Spin-Flop Coupling to Collinear Spin Alignment in Antiferromagnetic/ferromagnetic Nanostructures. *Nano Lett* (2012) 12: 2386–90. doi:10.1021/nl300361e
10. Olsen FK, Hallsteinsen I, Arenholz E, Tybell T, Folven E. Coexisting Spin-Flop Coupling and Exchange Bias in LaFeO3/La0.7Sr0.3MnO3 Heterostructures. *Phys Rev B* (2019) 99:134411. doi:10.1103/PhysRevB.99.134411
11. Malozemoff AP. Random-field Model of Exchange Anisotropy at Rough Ferromagnetic-Antiferromagnetic Interfaces. *Phys Rev B* (1987) 35:3679–82. doi:10.1103/PhysRevB.35.3679
12. Schulthess TC, Butler WH. Consequences of Spin-Flop Coupling in Exchange Biased Films. *Phys Rev Lett* (1998) 81:4516–9. doi:10.1103/physrevlett.81.4516
13. Dong S, Yamauchi K, Yunoki S, Yu R, Liang S, Moreo A, et al. Exchange Bias Driven by the Dzyaloshinskii-Moriya Interaction and Ferroelectric Polarization at G-type Antiferromagnetic Perovskite Interfaces. *Phys Rev Lett* (2009) 103:127201. doi:10.1103/PhysRevLett.103.127201
14. Yu P, Lee J-S, Okamoto S, Rossell MD, Huijben M, Yang C-H, et al. Interface Ferromagnetism and Orbital Reconstruction in BiFeO3–La0.7Sr0.3MnO3 Heterostructures. *Phys Rev Lett* (2010) 105:027201. doi:10.1103/PhysRevLett.105.027201
15. Huijben M, Yu P, Martin LW, Molegraaf HJA, Chu Y-H, Holcomb MB, et al. Ultrathin Limit of Exchange Bias Coupling at Oxide Multiferroic/ferromagnetic Interfaces. *Adv Mater* (2013) 25:4739–45. doi:10.1002/adma.201300940
16. Vafaee M, Finizio S, Deniz H, Zabel H, Jakob G, Kläui M. The Effect of Interface Roughness on Exchange Bias in La0.7Sr0.3MnO3-BiFeO3 Heterostructures. *Appl Phys Lett* (2016) 108:072401. doi:10.1063/1.4941795
17. Neumann RF, Bahiana M, Binggeli N. Magnetic Properties of La0.67Sr0.33MnO3/BiFeO3(001) Heterojunctions: Chemically Abrupt vs. Atomic Intermixed Interface. *EPL* (2012) 100:67002. doi:10.1209/0295-5075/100/67002
18. Nakagawa N, Hwang HY, Muller DA. Why Some Interfaces Cannot Be Sharp. *Nat Mater* (2006) 5:204–9. doi:10.1038/nmat1569
19. Chambers SA, Engelhard MH, Shutthanandan V, Zhu Z, Droubay TC, Qiao L, et al. Instability, Intermixing and Electronic Structure at the Epitaxial LaAlO3/SrTiO3(001) Heterojunction. *Surf Sci Rep* (2010) 65:317–52. doi:10.1016/j.surfrep.2010.09.001
20. Choi WS, Rouleau CM, Seo SSA, Luo Z, Zhou H, Fister TT, et al. Atomic Layer Engineering of Perovskite Oxides for Chemically Sharp Heterointerfaces. *Adv Mater* (2012) 24:6423–8. doi:10.1002/adma.201202691
21. Willmott PR, Pauli SA, Herger R, Schlepütz CM, Martoccia D, Patterson BD, et al. Structural Basis for the Conducting Interface between LaAlO3 and SrTiO3. *Phys Rev Lett* (2007) 99:155502. doi:10.1103/PhysRevLett.99.155502
22. May SJ, Shah AB, te Velthuis SGE, Fitzsimmons MR, Zuo JM, Zhai X, et al. Magnetically Asymmetric Interfaces in a LaMnO3/SrMnO3 superlattice Due to Structural Asymmetries. *Phys Rev B* (2008) 77:174409. doi:10.1103/PhysRevB.77.174409
23. Chambers SA, Qiao L, Droubay TC, Kaspar TC, Arey BW, Sushko PV. Band Alignment, Built-In Potential, and the Absence of Conductivity at the LaCrO3/SrTiO3(001) Heterojunction. *Phys Rev Lett* (2011) 107:206802. doi:10.1103/PhysRevLett.107.206802
24. Gibert M, Viret M, Torres-Pardo A, Piamonteze C, Zubko P, Jaouen N, et al. Interfacial Control of Magnetic Properties at LaMnO3/LaNiO3 Interfaces. *Nano Lett* (2015) 15:7355–61. doi:10.1021/acs.nanolett.5b02720
25. Hawthorn DG, He F, Venema L, Davis H, Achkar AJ, Zhang J, et al. An In-Vacuum Diffractometer for Resonant Elastic Soft X-ray Scattering. *Rev Scientific Instr* (2011) 82:073104. doi:10.1063/1.3607438
26. Solovyev I, Hamada N, Terakura K. Crucial Role of the Lattice Distortion in the Magnetism of LaMnO3. *Phys Rev Lett* (1996) 76:4825–8. doi:10.1103/PhysRevLett.76.4825
27. Wang XR, Li CJ, Lü WM, Paudel TR, Leusink DP, Hoek M, et al. Imaging and Control of Ferromagnetism in LaMnO3/SrTiO3 Heterostructures. *Science* (2015) 349:716–9. doi:10.1126/science.aaa5198
28. Niu W, Liu W, Gu M, Chen Y, Zhang X, Zhang M, et al. Direct Demonstration of the Emergent Magnetism Resulting from the Multivalence Mn in a LaMnO3 Epitaxial Thin Film System. *Adv Electron Mater* (2018) 4:1800055. doi:10.1002/aelm.201800055
29. Li M, Tang C, Paudel TR, Song D, Lü W, Han K, et al. Controlling the Magnetic Properties of LaMnO3/SrTiO3 Heterostructures by Stoichiometry and

Electronic Reconstruction: Atomic-Scale Evidence. *Adv Mater* (2019) 31: 1901386. doi:10.1002/adma.201901386
30. Chen B, Gauquelin N, Reith P, Halisdemir U, Jannis D, Spreitzer M, et al. Thermal-strain-engineered Ferromagnetism of LaMnO3/SrTiO3 Heterostructures Grown on Silicon. *Phys Rev Mater* (2020) 4:024406. doi:10.1103/physrevmaterials.4.024406
31. Scholl A, Stöhr J, Lüning J, Seo JW, Fompeyrine J, Siegwart H, et al. Observation of Antiferromagnetic Domains in Epitaxial Thin Films. *Science* (2000) 287:1014–6. doi:10.1126/science.287.5455.1014
32. Xu P, Han W, Rice PM, Jeong J, Samant MG, Mohseni K, et al. Reversible Formation of 2D Electron Gas at the LaFeO3 /SrTiO3 Interface via Control of Oxygen Vacancies. *Adv Mater* (2017) 29:1604447. doi:10.1002/adma.201604447
33. Izumi M, Murakami Y, Konishi Y, Manako T, Kawasaki M, Tokura Y. Structure Characterization and Magnetic Properties of Oxide superlattices La0.6Sr0.4MnO3/La0.6Sr0.4FeO3. *Phys Rev B* (1999) 60:1211–5. doi:10.1103/PhysRevB.60.1211
34. Anahory Y, Embon L, Li CJ, Banerjee S, Meltzer A, Naren HR, et al. Emergent Nanoscale Superparamagnetism at Oxide Interfaces. *Nat Commun* (2016) 7: 12566. doi:10.1038/ncomms12566
35. Smolin SY, Choquette AK, Wilks RG, Gauquelin N, Félix R, Gerlach D, et al. Energy Level Alignment and Cation Charge States at the LaFeO3/LaMnO3(001) Heterointerface. *Adv Mater Inter* (2017) 4:1700183. doi:10.1002/admi.201700183
36. Kourkoutis LF, Muller DA, Hotta Y, Hwang HY. Asymmetric Interface Profiles in LaVO3/SrTiO3 Heterostructures Grown by Pulsed Laser Deposition. *Appl Phys Lett* (2007) 91:163101. doi:10.1063/1.2798060
37. Ahn KH, Wu XW, Liu K, Chien CL. Magnetic Properties and Colossal Magnetoresistance of La(Ca)MnO3 materials Doped with Fe. *Phys Rev B* (1996) 54:15299–302. doi:10.1103/PhysRevB.54.15299
38. Chen Z, Chen Z, Liu ZQ, Holtz ME, Li CJ, Wang XR, et al. Electron Accumulation and Emergent Magnetism in LaMnO3/SrTiO3 Heterostructures. *Phys Rev Lett* (2017) 119:156801. doi:10.1103/PhysRevLett.119.156801
39. Chen B, Gauquelin N, Jannis D, Cunha DM, Halisdemir U, Piamonteze C, et al. Strain-Engineered Metal-to-Insulator Transition and Orbital Polarization in Nickelate Superlattices Integrated on Silicon. *Adv Mater* (2020) 32:2004995. doi:10.1002/adma.202004995
40. Nakamura M, Kagawa F, Tanigaki T, Park HS, Matsuda T, Shindo D, et al. Spontaneous Polarization and Bulk Photovoltaic Effect Driven by Polar Discontinuity in LaFeO3/SrTiO3 Heterojunctions. *Phys Rev Lett* (2016) 116:156801. doi:10.1103/PhysRevLett.116.156801
41. Goodenough JB. Theory of the Role of Covalence in the Perovskite-type Manganites[La, M(II)]MnO3. *Phys Rev* (1955) 100:564–73. doi:10.1103/PhysRev.100.564
42. Kanamori J. Superexchange Interaction and Symmetry Properties of Electron Orbitals. *J Phys Chem Sol* (1959) 10:87–98. doi:10.1016/0022-3697(59)90061-7
43. Goodenough JB, Wold A, Arnott RJ, Menyuk N. Relationship between Crystal Symmetry and Magnetic Properties of Ionic Compounds Containing Mn3+. *Phys Rev* (1961) 124:373–84. doi:10.1103/PhysRev.124.373
44. De K, Ray R, Narayan Panda R, Giri S, Nakamura H, Kohara T. The Effect of Fe Substitution on Magnetic and Transport Properties of LaMnO3. *J Magnetism Magn Mater* (2005) 288:339–46. doi:10.1016/j.jmmm.2004.09.118
45. Wu L, Li C, Chen M, Zhang Y, Han K, Zeng S, et al. Interface-Induced Enhancement of Ferromagnetism in Insulating LaMnO3 Ultrathin Films. *ACS Appl Mater Inter* (2017) 9:44931–7. doi:10.1021/acsami.7b15364

Conflict of Interest: The authors declare that the research was conducted in the absence of any commercial or financial relationships that could be construed as a potential conflict of interest.

Publisher's Note: All claims expressed in this article are solely those of the authors and do not necessarily represent those of their affiliated organizations, or those of the publisher, the editors and the reviewers. Any product that may be evaluated in this article, or claim that may be made by its manufacturer, is not guaranteed or endorsed by the publisher.